ACS ORGANIC & INORGANIC Au
AN OPEN ACCESS JOURNAL OF THE AMERICAN CHEMICAL SOCIETY

pubs.acs.org/orginorgau
Article

High-Density Formation of Ir/MoO_x Interface through Hybrid Clustering for Chemoselective Nitrostyrene Hydrogenation

Shun Hayashi* and Tetsuya Shishido

Cite This: ACS Org. Inorg. Au 2023, 3, 283−290
Read Online

ACCESS | Metrics & More | Article Recommendations | Supporting Information

ABSTRACT: To form high-density metal/oxide interfacial active sites, we developed a catalyst preparation method based on hybrid clustering. An iridium−molybdenum (Ir−Mo) hybrid clustering catalyst was prepared by using the hybrid cluster $[(IrCp^*)_4Mo_4O_{16}]$ ($Cp^* = \eta^5$-C_5Me_5) as the precursor. The Ir−Mo hybrid clustering catalyst selectively reduced the nitro group in the hydrogenation of 4-nitrostyrene, whereas the coimpregnated Ir−Mo catalyst reduced both the nitro and vinyl groups nonselectively. The hybrid clustering catalyst also exhibited high selectivity, even at a high Ir loading (5 wt %), in contrast to Ir/MoO_3, which exhibited high selectivity only at low Ir loadings (<0.3 wt %). In situ X-ray absorption spectroscopy analysis revealed that oxygen vacancies were formed at the Ir/MoO_x interface in the presence of H_2. We concluded that a high-density Ir/MoO_x interface contributes to the preferential adsorption of nitro groups on vacant sites, promoting the selective hydrogenation of nitro groups.

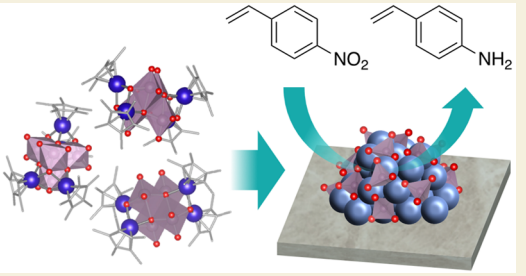

KEYWORDS: *nitrostyrene hydrogenation, organometallic polyoxometalate, nanoparticle, iridium, molybdenum, interface*

1. INTRODUCTION

Supported metal nanoparticles composed of platinum group metals (PGMs) such as Ru, Rh, Pd, and Pt are widely used as catalysts for hydrogenation because of their activity for dissociative adsorption of H_2 and the subsequent addition of the dissociated H atoms.[1] One of the most challenging problems for PGM catalysts is the control of selectivity in chemoselective hydrogenation, where more than one reducible functional group is present. For example, chemoselective hydrogenation of nitroarenes, an important process in the production of functionalized anilines, requires the development of catalysts that can selectively reduce the nitro group in the presence of other reducible groups such as C═C and C═O.[2−4] To enhance selectivity, considerable efforts have been made, including the formation of highly or atomically dispersed species,[5−8] confinement of nanoparticles within microporous supports,[9,10] introduction of a less active component,[11,12] surface modification through strong metal−support interaction (SMSI),[13,14] and surface decoration with an additional metal oxide component.[15−19] These approaches modulate the preferential adsorption of the nitro group through electronic or steric effects, resulting in selective hydrogenation of the nitro group. Therefore, the formation of a high density of metal/oxide interfacial sites is key to enhancing selectivity.

A straightforward strategy for the efficient formation of metal/oxide interfacial sites is to prepare the catalyst from a PGM precursor with such interfaces. We focused on the possibility of preparing catalysts by using hybrid clustering. Hybrid clusters or organometallic polyoxometalates, formulated as $[(M^1L)_xM^2_yO_n]$, are composed of metal ions (M^1), metal oxide clusters ($M^2_yO_n$), and organic ligands (L).[20] Because the surface oxygen atoms of the metal oxide clusters are coordinated to the metal ions, the hybrid clusters can be viewed as minimal building blocks with M^1−O−M^2 interfaces. Therefore, we expected the catalysts prepared from the hybrid clusters to have a high density of metal/oxide interfaces, contributing to chemoselective hydrogenation. We previously reported that PGM-based hybrid clustering catalysts exhibited improved activity compared to the corresponding coimpregnated catalysts.[21,22] Despite the potential of hybrid clustering catalysts in various applications, there have been few reports on their use in heterogeneous catalysts.[23,24]

In this study, Ir-M-based hybrid clustering catalysts (M = Mo, V) were prepared by using hybrid clusters $[(IrCp^*)_4Mo_4O_{16}]$ and $[(IrCp^*)_4V_6O_{19}]$ ($Cp^* = \eta^5$-C_5Me_5) as the precursors (Figure 1). The effect of the preparation method on the catalytic performance was tested using the hydrogenation of 4-nitrostyrene as a model reaction. The formation mechanism of the Ir/MO_x interface was studied by using in situ X-ray absorption spectroscopy (XAS). The effect

Received: May 5, 2023
Revised: June 30, 2023
Accepted: June 30, 2023
Published: July 13, 2023

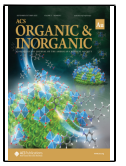

https://doi.org/10.1021/acsorginorgau.3c00017
ACS Org. Inorg. Au 2023, 3, 283−290

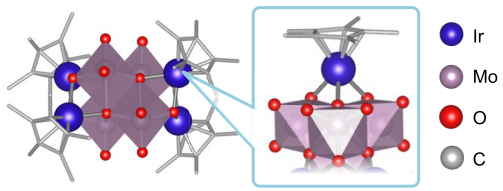

Figure 1. $[(IrCp^*)_4Mo_4O_{16}]$ as a catalyst precursor with Ir−O−Mo interfaces. Hydrogen atoms have been omitted for clarity.

of the Ir/MO_x interface on the selectivity is evaluated through in situ XAS and kinetic studies.

2. RESULTS AND DISCUSSION

2.1. Preparation of Hybrid Clustering Catalyst

The hybrid clustering catalysts, Ir_4Mo_4/Al_2O_3 and Ir_4V_6/Al_2O_3, were prepared by using $[(IrCp^*)_4Mo_4O_{16}]$ and $[(IrCp^*)_4V_6O_{19}]$ as the catalyst precursors, respectively. These precursors were synthesized according to the procedures reported in previous studies[25,26] and characterized using positive-ion electrospray ionization mass spectrometry (ESI-MS) and Fourier transform infrared (FT-IR) spectroscopy (Figures S1 and S2). The most intense peaks in the positive-ion ESI mass spectra were assigned to the monovalent proton adducts $[H(IrCp^*)_4Mo_4O_{16}]^+$ and $[H(IrCp^*)_4V_6O_{19}]^+$. The FT-IR spectra exhibited characteristic absorption patterns corresponding to the desired clusters. After the precursor clusters were adsorbed on γ-Al_2O_3 by impregnation with methanol, the catalysts were prepared through calcination in air at 573 K, followed by reduction under a H_2 flow at 573 K. The coimpregnated Ir−Mo and Ir−V catalysts, Ir−Mo/Al_2O_3 and Ir−V/Al_2O_3 ([Mo]/[Ir] = 1, [V]/[Ir] = 1.5), and the pristine Ir catalyst, Ir/Al_2O_3, were prepared using H_2IrCl_6, $(NH_4)_6[Mo_7O_{24}]\cdot 4H_2O$, and NH_4VO_3 under identical calcination conditions.

According to high-angle annular dark-field scanning transmission electron microscopy (HAADF-STEM) analysis, the average diameters of Ir_4Mo_4/Al_2O_3 and Ir−Mo/Al_2O_3 were estimated as 1.2 ± 0.2 and 1.3 ± 0.3 nm, respectively, indicating that small nanoparticles were formed regardless of the preparation method (Figure 2).

The electronic and local structures of Ir_4Mo_4/Al_2O_3 and Ir−Mo/Al_2O_3 were studied through Ir L_3- and Mo K-edge XAS. The white-line intensities of the Ir L_3-edge X-ray absorption near-edge structure (XANES) spectra were used to determine the oxidation state of Ir. The intensity of Ir_4Mo_4/Al_2O_3 was lower than that of Ir−Mo/Al_2O_3, indicating that the Ir species

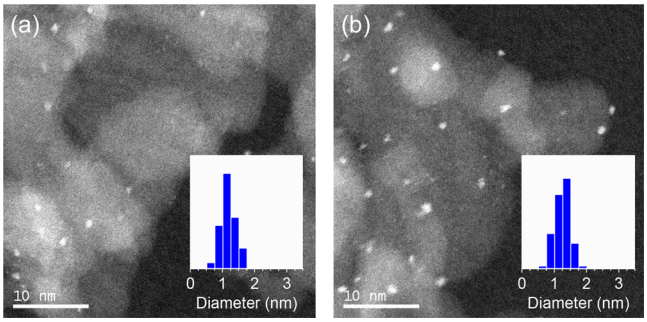

Figure 2. HAADF-STEM images of (a) Ir_4Mo_4/Al_2O_3 and (b) Ir−Mo/Al_2O_3.

in Ir_4Mo_4/Al_2O_3 were relatively reduced (Figure 3a). The Fourier transform of extended X-ray absorption fine structure

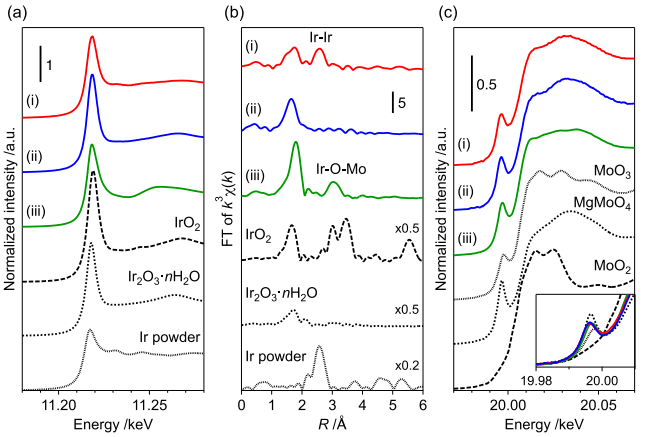

Figure 3. Ir L_3-edge (a) XANES, (b) FT-EXAFS, and (c) Mo K-edge XANES spectra of (i) Ir_4Mo_4/Al_2O_3, (ii) Ir−Mo/Al_2O_3, and (iii) $[(IrCp^*)_4Mo_4O_{16}]$.

(FT-EXAFS) was analyzed by curve-fitting the inverse Fourier transform of the EXAFS spectra. The peak derived from the second coordination sphere of $[(IrCp^*)_4Mo_4O_{16}]$ is assigned to Mo (Figures 3b and S3, Table S1). This is consistent with the crystal structure in which the surface oxygen atoms in the Mo_4O_{16} unit are coordinated to the Ir atoms.[25] In contrast, the peak derived from the second coordination sphere of Ir_4Mo_4/Al_2O_3 is assigned to Ir. The bond length (2.69 Å) was almost equal to that of the Ir powder (2.71 Å), indicating the presence of metallic Ir species. Although Ir is intrinsically prone to reoxidation upon exposure to air after reduction, metallic species are preserved in Ir_4Mo_4/Al_2O_3. Therefore, we concluded that a core−shell structure was formed on Ir_4Mo_4/Al_2O_3, where the metallic Ir core was covered with an Ir−Mo mixed oxide shell. In the case of coimpregnated Ir−Mo/Al_2O_3, no peaks derived from the second coordination sphere were observed. Because the white-line intensity of the XANES spectrum and the oscillation pattern of the EXAFS spectrum matched well with those of $Ir_2O_3\cdot nH_2O$, we conclude that Ir_2O_3 nanoparticles were formed on Ir−Mo/Al_2O_3.

The pre-edge peaks in the Mo K-edge XANES spectra were assigned to weak quadrupole-allowed (1s → 4d) and strong dipole-allowed (1s → 5p) transitions, and the local structural disorder of the Mo oxide species reflected the intensity.[27,28] The Mo K-edge XANES spectrum of Ir_4Mo_4/Al_2O_3 matched well with that of Ir−Mo/Al_2O_3, indicating that the local structure of Mo was independent of the preparation method (Figure 3c).

2.2. Hydrogenation of 4-Nitrostyrene

The catalytic activities were tested through the chemoselective hydrogenation of 4-nitrostyrene (**1**) to 4-aminostyrene (**2**). The substrate had two reducible groups, and the desired product (**2**) was obtained via the selective hydrogenation of the nitro group. The reaction also afforded two byproducts: 4-nitroethylbenzene (**3**), formed by the selective hydrogenation of the vinyl group, and 4-aminoethylbenzene (**4**), formed after complete hydrogenation (Scheme 1). In the initial stage of the reaction, Ir_4Mo_4/Al_2O_3 selectively reduced the nitro group to produce **2** (select. > 96%, conv. < 48%) (Figure 4a). In contrast, Ir−Mo/Al_2O_3 nonselectively reduced both the nitro

https://doi.org/10.1021/acsorginorgau.3c00017
ACS Org. Inorg. Au 2023, 3, 283−290

Scheme 1. Hydrogenation of 4-Nitrostyrene (1)

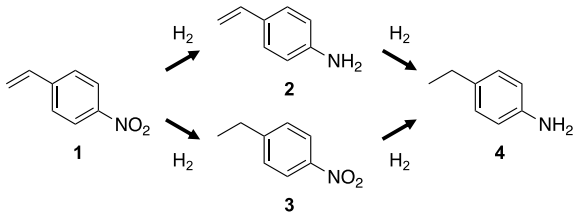

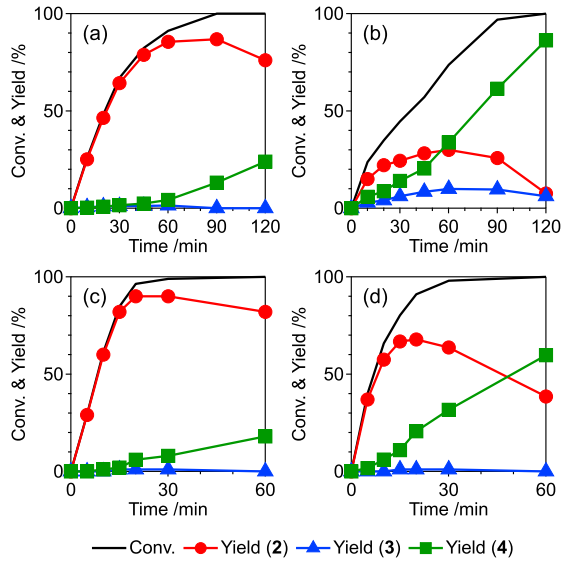

Figure 4. Time courses of the hydrogenation of **1** catalyzed by (a) Ir_4Mo_4/Al_2O_3, (b) Ir−Mo/Al_2O_3, (c) Ir_4Mo_4/TiO_2, and (d) Ir−Mo/TiO_2. Reaction conditions: **1** (0.1 mmol), H_2 (0.3 MPa), toluene (1 mL), catalyst (10 mg, Ir: 0.52 mol %), and 303 K.

and C═C groups, and the selectivity toward **2** reached 63% (Figure 4b). The optimized hybrid clustering catalyst with a TiO_2 support, Ir_4Mo_4/TiO_2, prepared through calcination at 573 K, followed by H_2 reduction at 773 K, exhibited higher activity and selectivity in comparison to the catalyst with an Al_2O_3 support (Figure 4c). Although the Al_2O_3-supported catalysts had little influence on the reduction temperature, the TiO_2-supported catalysts at a reduction temperature of 773 K exhibited selectivity higher than that at 573 K (Table S2). This is probably due to the reducible nature of TiO_2, which results in the formation of an Ir/TiO_x interface via SMSI.[13,14] The formation of Ir/TiO_x contributes to the selectivity by the preferential adsorption of the nitro group and the encapsulation of nonselective Ir−Ir sites.[29,30] Ir_4Mo_4/TiO_2 exhibited a high initial selectivity (>99%, conv. < 61%) and maintained its selectivity during the later stages of the reaction (select. 94%, conv. 97%). Although the corresponding coimpregnated catalyst, Ir−Mo/TiO_2, also exhibited improved activity and selectivity compared to the Al_2O_3-supported catalyst, the selectivity significantly decreased as the conversion exceeded ~70% (Figure 4d). These results suggest that Ir/MoO_x is more selective than Ir/TiO_x and that the selectivity of the hybrid clustering catalyst can be improved by optimization of the support.

Enhanced selectivity through hybrid clustering has also been observed for other oxide species such as V. The hybrid clustering Ir−V catalyst, Ir_4V_6/Al_2O_3, also exhibited higher selectivity than the coimpregnated Ir−V catalyst, Ir−V/Al_2O_3; however, the introduction of Mo was more effective than that of V, regardless of the preparation method (Figure 5a, Table S3). A general and straightforward formation method of an Ir/MoO_x interface is to deposit the Ir species onto a Mo-oxide support with a high dispersion. Single-atom catalysts (SACs) have demonstrated unique activities in a variety of reactions, including nitrostyrene hydrogenation.[5,31] Low metal loadings (e.g., 0.1 wt %) are required to achieve SAC through inhibiting aggregation. To examine the effect of loading on selectivity, the activity of Ir_4Mo_4/Al_2O_3 was compared with that of an Ir catalyst supported on MoO_3, Ir/MoO_3. Ir/MoO_3 exhibited high selectivity with low (<0.3 wt %) Ir loadings (Figure 5b). However, the selectivity decreased significantly when the loading increased, probably because of the formation of aggregated Ir species. In contrast, Ir_4Mo_4/Al_2O_3 exhibited high selectivity even at a high Ir loading (5 wt %) (Figure 5c). These results indicate that the formation of the Ir/MoO_x interface is the key to chemoselective hydrogenation, regardless of the catalyst preparation method, and that hybrid clustering is an efficient method to form such interfacial sites exclusively.

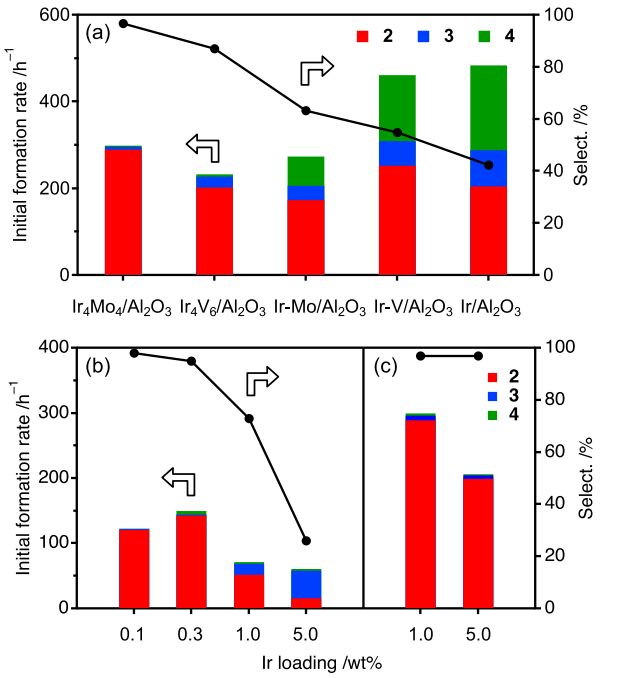

Figure 5. Initial reaction rate of the hydrogenation of **1** over (a) Ir−Mo- and Ir−V-based catalysts, (b) Ir/MoO_3, and (c) Ir_4Mo_4/Al_2O_3 with different Ir loadings. Reaction conditions were identical to those cited in the caption of Figure 4 except for the catalyst amount (2−100 mg, Ir: 0.52 mol %). The original data are summarized in Table S3.

2.3. Formation Mechanism of Ir/MoO_x Interface

The high selectivity of Ir_4Mo_4/Al_2O_3 was observed only when the catalyst was prepared via calcination in air and subsequent reduction under a H_2 flow. The optimal temperature for both aerobic calcination and H_2 reduction was 573 K for the Al_2O_3-supported catalyst. The catalysts prepared through calcination at varying temperatures followed by H_2 reduction at 573 K exhibited increased selectivity with increasing calcination temperature, reaching a maximum at 573 K (Figure 6a). Subsequently, the selectivity decreased with a further increase in the calcination temperature. In contrast, the effect of the

https://doi.org/10.1021/acsorginorgau.3c00017
ACS Org. Inorg. Au 2023, 3, 283−290

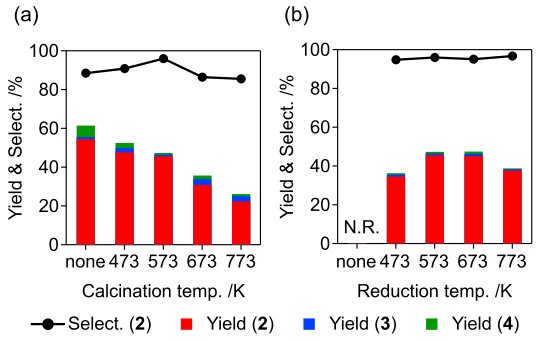

Figure 6. Effect of the preparation conditions on the activity of Ir_4Mo_4/Al_2O_3 prepared through (a) calcination at varying temperatures followed by H_2 reduction at 573 K and (b) calcination at 573 K followed by H_2 reduction at varying temperatures. Reaction conditions were identical with those cited in the caption of Figure 4 except for the reaction time (20 min).

reduction temperature on activity was relatively low (Figure 6b).

To elucidate the formation mechanism of active sites on Ir_4Mo_4/Al_2O_3 through thermal treatment, in situ XANES analysis was conducted under two conditions: (i) calcination of the adsorbed cluster Ir_4Mo_4/Al_2O_3_ads under 20% O_2/He flow, and (ii) reduction of the calcined catalyst Ir_4Mo_4/Al_2O_3_air(573) under H_2 flow (Figure S4). The measurements were conducted at 303 K and thereafter at temperatures ranging from 373 to 773 K in increments of 100 K. The white-line intensity of the Ir L_3-edge spectra was determined from the maximum normalized absorbance and was used as a measure of the oxidation state of Ir (Figure 7a). Similarly, the edge

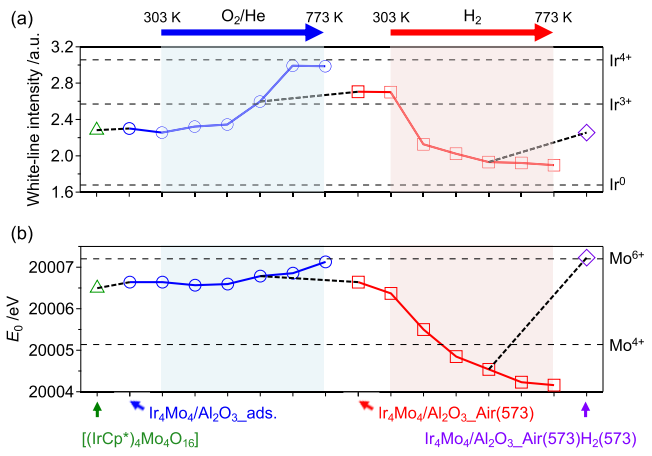

Figure 7. Oxidation states of Ir and Mo during calcination and reduction. (a) White-line intensity of the Ir L_3-edge XANES spectra. (b) Edge energy (E_0) of the Mo K-edge XANES spectra. The original XANES spectra are shown in Figure S4.

energy (E_0) of the Mo K-edge spectra was determined from the second peak of the first derivative of the normalized absorbance and used as a measure of the oxidation state of Mo (Figure 7b). These intensities and energies increased with increasing oxidation states, as observed for the reference samples of Ir (Ir powder, $Ir_2O_3 \cdot nH_2O$, and IrO_2 for Ir^0, Ir^{3+}, and Ir^{4+}, respectively) and Mo (MoO_2 and MoO_3 for Mo^{4+} and Mo^{6+}, respectively).

During calcination under a 20% O_2/He flow up to 573 K, no significant changes in the oxidation states of Ir and Mo were observed. The oxidation of Ir began at 573 K and a slight change in the oxidation state of Mo was observed. Further increase in the calcination temperature resulted in the formation of Ir^{4+}. Thermogravimetry-differential thermal analysis (TG-DTA) of $[(IrCp^*)_4Mo_4O_{16}]$ under an air flow indicated a weight loss (29.5%) at temperatures ranging from 543 to 599 K (Figure S5). This is attributed to the removal of the Cp* ligand and the reduction of Ir^{3+} to Ir^+ (theoretical value of 29.4%). Thereafter, a gradual weight increase (4.3%) was observed, which was attributed to the oxidation of Ir^+ to Ir^{4+} (theoretical value of 4.9%). Therefore, we concluded that the increase in the oxidation state of Ir and Mo is derived from the decomposition of the precursor cluster and the calcination temperature of 573 K is the minimum temperature required to remove organic ligands without further oxidation. As described previously, the selectivity of Ir_4Mo_4/Al_2O_3 was significantly affected by the calcination temperature, and high selectivity was observed only at 573 K (Figure 6a). The organic ligand remained at a lower calcination temperature, and further oxidation proceeded at a higher calcination temperature, resulting in a decrease in the selectivity of the catalyst.

During reduction under a H_2 flow, reductions in both Ir and Mo were observed. Selectivity was not significantly affected by the reduction temperature; however, the reduction process was found to be essential for activity (Figure 6b). Ex situ analysis of the optimized catalyst, Ir_4Mo_4/Al_2O_3_air(573) H_2 (573), revealed that the catalyst was reoxidized after exposure to air (Figures 3 and 7). These results indicate that both the reduction and reoxidation processes contribute to the formation of surface Ir/MoO_x interfacial sites.

2.4. Role of Ir/MoO_x Interface on the Catalytic Performance

To determine the effect of the Ir/MoO_x interface on selectivity, in situ XAS analysis of the catalysts under a H_2 flow was conducted (Figure S6). According to the Ir L_3-edge XANES spectra, a reduction of Ir was observed for both Ir_4Mo_4/Al_2O_3 and Ir–Mo/Al_2O_3 upon exposure to H_2 (Figure 8a). In contrast, according to the Mo K-edge XANES spectra,

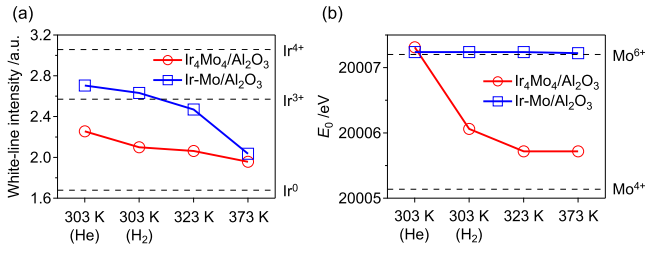

Figure 8. Oxidation states of Ir and Mo under a H_2 atmosphere. (a) White-line intensity of Ir L_3-edge XANES spectra. (b) Edge energy (E_0) of the Mo K-edge XANES spectra. The original XANES spectra are shown in Figure S6.

the reduction of Mo in Ir_4Mo_4/Al_2O_3 was observed even at 303 K, whereas the oxidation state of Mo in Ir–Mo/Al_2O_3 was retained (Figure 8b). The reduction of both Ir and Mo indicates that oxygen vacancies were formed at the Ir/MoO_x interface of Ir_4Mo_4/Al_2O_3 in the presence of H_2. As reported for MoO_3-supported or MoO_x-modified metal catalysts for deoxygenation[32,33] and chemoselective hydrogenation,[16,19,34,35] the presence of Mo results in the preferential adsorption of oxygen-containing functional groups. This is because of the reducible nature of Mo, which affects its

https://doi.org/10.1021/acsorginorgau.3c00017
ACS Org. Inorg. Au 2023, 3, 283–290

adsorption behavior through the formation of oxygen vacancies or electronic interactions with the metal species.

To determine how the formation of oxygen vacancies contributes to improved selectivity, kinetic studies on the hydrogenation of nitrobenzene (NB) and styrene (ST) were conducted (Scheme 2). The hydrogenation of NB and ST

Scheme 2. Hydrogenation of (a) Nitrobenzene and (b) Styrene[a]

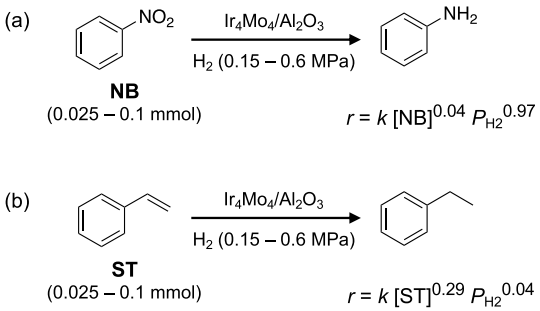

[a]The reaction orders were estimated based on the kinetic studies (Figure S7).

afforded aniline and ethylbenzene as the only products, respectively. The reaction order with respect to the concentration of the substrate ([NB] or [ST]) and the hydrogen pressure (P_{H2}) was estimated from the initial reaction rate under different reaction conditions (Figure S7). For the hydrogenation of NB, the reaction orders with respect to [NB] and P_{H2} were estimated as 0.04 and 0.97, respectively (Scheme 2a, Table S4). The zero-order kinetics with respect to [NB] indicates that the adsorption of NB is not involved in the rate-determining step (RDS) and that the RDS is a H_2-involved step, such as the formation of an oxygen vacancy or the hydrogenation of adsorbed NB. The efficient adsorption of NB can be explained by the formation of oxygen vacancies, where oxygen-containing functional groups are preferentially adsorbed. In contrast, the reaction orders with respect to [ST] and P_{H2} were estimated as 0.29 and 0.04, respectively, for the hydrogenation of ST (Scheme 2b). This indicates that hydrogen adsorption is not related to the RDS and that the RDS is an ST-involved step, such as the adsorption of ST or the hydrogenation of adsorbed ST. The kinetics of the hydrogenation on coimpregnated Ir−Mo/Al_2O_3 was completely different from that on Ir_4Mo_4/Al_2O_3. Regardless of the substrate (NB or ST), the reaction orders with respect to the substrate were between 0 and 1 and those to P_{H2} were almost 1 (Figure S8 and Table S4). This implies that the hydrogenation of NB and ST on Ir−Mo/Al_2O_3 proceeded by a similar mechanism and that the RDS is the reduction of the adsorbed substrate by the hydrogen. The hydrogenation of ST was conducted in the presence of NB to understand the competitive behavior of chemoselective hydrogenation (Figure 9). For Ir_4Mo_4/Al_2O_3, ST hydrogenation was completely suppressed in the presence of NB. This is in contrast to Ir−Mo/Al_2O_3, where ST hydrogenation proceeded in the presence of NB. Moreover, the reaction rates of the separate ST and NB hydrogenations were comparable over Ir−Mo/Al_2O_3.

Regarding the effect of the Ir/MoO_x interface on the catalytic performance, we anticipate that selectivity is influenced by the preferential adsorption of nitro groups on

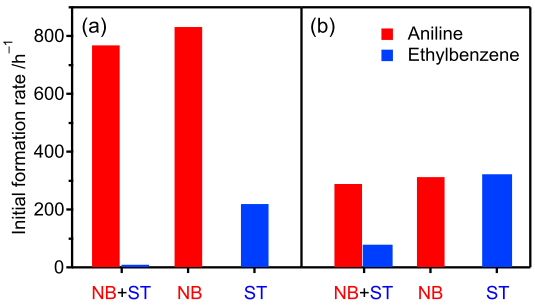

Figure 9. Initial reaction rate of the hydrogenation of the mixture (NB+ST), NB, and ST over (a) Ir_4Mo_4/Al_2O_3 and (b) Ir−Mo/Al_2O_3. Reaction conditions were identical to those cited inthe caption of Figure 4 except for the substrates.

the oxygen vacancies formed in the presence of H_2 (Figure 10). The vacant sites capture and reduce nitro groups rather

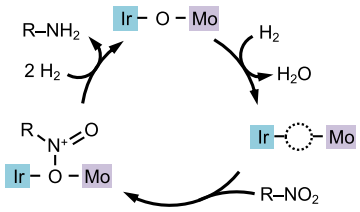

Figure 10. Plausible reaction mechanism of hydrogenation of nitroarene on Ir/MoO_x interfacial sites.

than vinyl groups and promote the subsequent hydrogenation process to produce anilines. This mechanism is consistent with that of reported PGM catalysts having interfacial active sites with reducible metal oxides.[18,36]

3. CONCLUSIONS

In this study, an Ir−Mo-based catalyst, Ir_4Mo_4/Al_2O_3, was prepared by using an Ir−Mo hybrid cluster $[(RhCp^*)_4Mo_4O_{16}]$ ($Cp^* = \eta^5$-C_5Me_5) as a precursor and applied as a catalyst for the hydrogenation of 4-nitrostyrene. Ir_4Mo_4/Al_2O_3 selectively reduced the nitro groups to produce 4-aminostyrene, whereas the coimpregnated catalyst, Ir−Mo/Al_2O_3, reduced both the nitro and vinyl groups nonselectively. Ir_4Mo_4/Al_2O_3 exhibited high selectivity even at a high Ir loading (5 wt %). This is in contrast to Ir/MoO_3, which exhibited high selectivity only when the loading was low (<0.3 wt %). The thermal treatment conditions used to prepare Ir_4Mo_4/Al_2O_3 strongly affected selectivity. The catalyst should be prepared through calcination in air at a minimal temperature to remove the organic ligands (Cp*) while preventing further oxidation of Ir. Subsequent reduction under H_2 is necessary for the catalyst to work effectively, and reoxidation by exposure to air is expected to play an important role in the formation of the Ir/MoO_x interface. In situ XAS analysis under H_2 revealed the reduction of Mo for Ir_4Mo_4/Al_2O_3 even at 303 K, which is explained by the formation of oxygen vacancies at the Ir/MoO_x interface. Oxygen vacancies preferentially adsorbed nitro groups over vinyl groups, thereby promoting selective hydrogenation of the nitro groups.

https://doi.org/10.1021/acsorginorgau.3c00017
ACS Org. Inorg. Au 2023, 3, 283−290

4. EXPERIMENTAL SECTION

4.1. Chemicals

Pentamethylcyclopentadienyl iridium(III) dichloride dimer, 4-nitrostyrene, and styrene were purchased from TCI. Hydrogen hexachloroiridate(IV) *n*-hydrate, ammonium molybdate(VI) tetrahydrate, disodium molybdate(VI) dihydrate, ammonium metavanadate, molybdenum(VI) oxide, and nitrobenzene were purchased from Wako Chemicals. Sodium metavanadate was obtained from Sigma-Aldrich. γ-Al_2O_3 (JRC-ALO-8) and TiO_2 (JRC-TIO-17) were supplied by the Catalysis Society of Japan. Before use, γ-Al_2O_3 and TiO_2 were calcined under air at 773 K for 3 h. Deionized water (Milli-Q, >18 MΩ cm) was used in all the experiments.

4.2. Synthesis of Hybrid Clusters

$[(IrCp^*)_4Mo_4O_{16}]$ was synthesized according to a procedure reported in a previous study.[25] $Na_2MoO_4{\cdot}2H_2O$ (1.21 g, 5.00 mmol) was dissolved in water (3 mL), and $[IrCp^*Cl_2]_2$ (398 mg, 0.500 mmol) was added. Thereafter, the mixture was stirred for 3 h at 353 K. After the reaction, the mixture was concentrated by using a rotary evaporator, and the product was extracted by using dichloromethane (DCM). The DCM layer was washed with water, and the crude product was obtained by evaporating the solvent. The purified product was obtained via recrystallization from DCM/toluene (91% yield). IR (KBr pellets, cm^{-1}): 932, 910, 696, 642, 577, and 536.

$[(IrCp^*)_4V_6O_{19}]$ was synthesized according to a procedure reported in a previous study.[26] $NaVO_3$ (610 mg, 5.00 mmol) was added to water (20 mL) and the mixture was stirred for 1 h for complete dissolution. Thereafter, $[IrCp^*Cl_2]_2$ (398 mg, 0.500 mmol) was added, and the mixture was stirred for 3 h at room temperature. After the reaction, the mixture was concentrated using a rotary evaporator, and the product was extracted using DCM. The DCM layer was washed with water, and the crude product was obtained by evaporating the solvent. The purified product was obtained via recrystallization from DCM/toluene (96% yield). IR (KBr pellet, cm^{-1}): 941, 674, 559, and 499.

4.3. Catalyst Preparation

The hybrid clustering catalyst Ir_4Mo_4/Al_2O_3 was prepared as follows: $[(IrCp^*)_4Mo_4O_{16}]$ (12.7 mg, 6.51 μmol) was dissolved in methanol (20 mL), and the solution was added dropwise to a methanolic dispersion of the γ-Al_2O_3 support (493 mg in 40 mL). The mixture was stirred for 2 h and subsequently dried slowly at 373 K. The resulting solid was dried overnight at 333 K. The catalyst was calcined in static air at 573 K for 1 h, followed by reduction under a H_2 flow (10 mL/min) at 573 K for 1 h. The catalyst was stored in the air. Ir_4V_6/Al_2O_3 was prepared by using $[(IrCp^*)_4V_6O_{19}]$ as the precursor. Ir−Mo/Al_2O_3, Ir−V/Al_2O_3, and Ir/Al_2O_3 were prepared by using H_2IrCl_6, $(NH_4)_6[Mo_7O_{24}]{\cdot}4H_2O$, and NH_4VO_3. Water was used as a solvent instead of methanol. Ir/MoO_3 was prepared by using H_2IrCl_6 and MoO_3. The calculated loading amounts of Ir, Mo, and V were 1.0, 0.50, and 0.40 wt %, respectively ([Mo]/[Ir] = 1, [V]/[Ir] = 1.5).

4.4. Characterization

Positive-ion ESI-MS was conducted with a Shimadzu LCMS-9050. The samples were dissolved in dichloromethane/methanol and electrosprayed at a bias voltage of +4 kV. FT-IR analysis was conducted using a JASCO FT/IR-6100 in transmission mode. The sample was mixed well with KBr and pressed to form a pellet, which was subsequently used for analysis. HAADF-STEM analysis was performed using a JEOL JEM-ARM200F instrument. The samples were prepared by dropping an ethanolic dispersion of the catalyst onto a copper grid with a support membrane and evaporating the solvent. Ir L_3-edge and Mo K-edge XAS measurements were conducted using the BL01B1 beamline at SPring-8 of the Japan Synchrotron Radiation Research Institute. The incident X-ray beam was monochromated using a Si(111) or Si(311) double-crystal monochromator for the Ir L_3-edge and Mo K-edge measurements, respectively. The measurements were conducted in fluorescence mode using a 19-element Ge solid-state detector at room temperature. Reference samples were ground with boron nitride and pressed into pellets. In situ XAS measurements were conducted in transmission mode using ionization chambers. The pellet sample was placed in a temperature-controlled gas cell equipped with Kapton windows under a gas flow (20% of the mixture of O_2/He (50 mL/min) or H_2 (50 mL/min)). The temperature was increased from 303 to 373 K and thereafter to 773 K in steps of 100 K. The temperature was maintained for 10 min before each measurement. The XAS data were analyzed using the Rigaku REX2000 program. After background subtraction, the k^3-weighted χ spectrum within a k range of 3−17.5 $Å^{-1}$ was Fourier-transformed into an r space. Curve-fitting analysis was performed on the first (Ir−O) and second (Ir−Mo and Ir−Ir) coordination spheres. The phase shifts and backscattering amplitude functions of the Ir−O, Ir−Mo, and Ir−Ir bonds were extracted from $[(IrCp^*)_4Mo_4O_{16}]$[25] using the FEFF8 program[37] by setting σ^2 at 0.0036. TG-DTA was conducted using a HITACHI STA7300 TG analyzer. The sample was heated at 353 K for 30 min, and the temperature was increased to 873 K at a ramping rate of 10 K/min under an air flow (200 mL/min). Gas chromatography (GC) analysis was conducted using a Shimadzu GC-2025 gas chromatograph comprising a flame ionization detector equipped with an InertCap 5 capillary column (internal diameter of 0.25 mm and length of 30 m).

4.5. Catalytic Test

The typical procedure for the hydrogenation of 4-nitrostyrene is as follows. The catalyst (10 mg, 0.52 mol % Ir) was placed in a glass tube, and 4-nitrostyrene (0.1 mmol) and toluene (1 mL) were subsequently added. Naphthalene (0.02 mmol) was also added as an internal standard. The glass tube was placed in an autoclave and H_2 was introduced. The reaction mixture was stirred at 303 K for a specified reaction time. After the reaction, the catalyst was filtered off and the filtrate was analyzed by GC. The conversion and yield were estimated based on the initial amounts of 4-nitrostyrene. The selectivity and the material balance were calculated according to the formulas below. The material balance was almost equal to 1 (0.95−1.05) in all experiments. The initial reaction rates were estimated from the yield of 4-aminostyrene divided by the product of the total amount of Ir and the reaction time. A representative GC chart of the reaction mixture is shown in Figure S9.

$$\text{selectivity to } \mathbf{2} = \frac{[\mathbf{2}]}{[\mathbf{2}] + [\mathbf{3}] + [\mathbf{4}]}$$

$$\text{material balance} = \frac{[\mathbf{1}] + [\mathbf{2}] + [\mathbf{3}] + [\mathbf{4}]}{[\mathbf{1}]_{\text{initial}}}$$

■ ASSOCIATED CONTENT

Data Availability Statement

The data underlying this study are available in the published article and its Supporting Information.

Supporting Information

The Supporting Information is available free of charge at https://pubs.acs.org/doi/10.1021/acsorginorgau.3c00017.

Results of characterization and catalytic test (PDF)

■ AUTHOR INFORMATION

Corresponding Author

Shun Hayashi − *Division of Physical Sciences, Department of Science and Engineering, National Museum of Nature and Science, Ibaraki 305-0005, Japan;* orcid.org/0000-0003-4832-3768; Email: s-hayashi@kahaku.go.jp

Author

Tetsuya Shishido − *Department of Applied Chemistry for Environment, Graduate School of Urban Environmental Sciences, Tokyo Metropolitan University, Tokyo 192−0397, Japan; Research Center for Hydrogen Energy−Based Society,*

Tokyo Metropolitan University, Tokyo 192-0397, Japan; Elements Strategy Initiative for Catalysts & Batteries, Kyoto University, Kyoto 615-8520, Japan; orcid.org/0000-0002-8475-4226

Complete contact information is available at: https://pubs.acs.org/10.1021/acsorginorgau.3c00017

Notes

The authors declare no competing financial interest.

■ ACKNOWLEDGMENTS

This research was financially supported by a Grant-in-Aid for Scientific Research (21K14463) from the Ministry of Education, Culture, Sports, Science, and Technology (MEXT). The HAADF-STEM analysis was conducted at the Advanced Characterization Nanotechnology Platform of the University of Tokyo supported by the Nanotechnology Platform of MEXT. The synchrotron radiation experiments were performed with the approval of the Japan Synchrotron Radiation Research Institute (JASRI) (2022B1655).

■ REFERENCES

(1) Vilé, G.; Albani, D.; Almora-Barrios, N.; López, N.; Pérez-Ramírez, J. Advances in the Design of Nanostructured Catalysts for Selective Hydrogenation. *ChemCatChem.* **2016**, *8*, 21−33.

(2) Blaser, H. U.; Steiner, H.; Studer, M. Selective Catalytic Hydrogenation of Functionalized Nitroarenes: An Update. *ChemCatChem.* **2009**, *1*, 210−221.

(3) Song, J.; Huang, Z. F.; Pan, L.; Li, K.; Zhang, X.; Wang, L.; Zou, J. J. Review on Selective Hydrogenation of Nitroarene by Catalytic, Photocatalytic and Electrocatalytic Reactions. *Appl. Catal. B Environ.* **2018**, *227*, 386−408.

(4) Coq, B.; Tijani, A.; Dutartre, R.; Figuéras, F. Influence of Support and Metallic Precursor on the Hydrogenation of P-Chloronitrobenzene over Supported Platinum Catalysts. *J. Mol. Catal.* **1993**, *79*, 253−264.

(5) Wei, H.; Liu, X.; Wang, A.; Zhang, L.; Qiao, B.; Yang, X.; Huang, Y.; Miao, S.; Liu, J.; Zhang, T. FeO_x-Supported Platinum Single-Atom and Pseudo-Single-Atom Catalysts for Chemoselective Hydrogenation of Functionalized Nitroarenes. *Nat. Commun.* **2014**, *5*, 5634.

(6) Zhang, S.; Chang, C. R.; Huang, Z. Q.; Li, J.; Wu, Z.; Ma, Y.; Zhang, Z.; Wang, Y.; Qu, Y. High Catalytic Activity and Chemoselectivity of Sub-Nanometric Pd Clusters on Porous Nanorods of CeO_2 for Hydrogenation of Nitroarenes. *J. Am. Chem. Soc.* **2016**, *138*, 2629−2637.

(7) Peng, Y.; Geng, Z.; Zhao, S.; Wang, L.; Li, H.; Wang, X.; Zheng, X.; Zhu, J.; Li, Z.; Si, R.; Zeng, J. Pt Single Atoms Embedded in the Surface of Ni Nanocrystals as Highly Active Catalysts for Selective Hydrogenation of Nitro Compounds. *Nano Lett.* **2018**, *18*, 3785−3791.

(8) Liu, W.; Feng, H.; Yang, Y.; Niu, Y.; Wang, L.; Yin, P.; Hong, S.; Zhang, B.; Zhang, X.; Wei, M. Highly-Efficient RuNi Single-Atom Alloy Catalysts toward Chemoselective Hydrogenation of Nitroarenes. *Nat. Commun.* **2022**, *13*, 3188.

(9) Zhang, J.; Wang, L.; Shao, Y.; Wang, Y.; Gates, B. C.; Xiao, F. S. A Pd@Zeolite Catalyst for Nitroarene Hydrogenation with High Product Selectivity by Sterically Controlled Adsorption in the Zeolite Micropores. *Angew. Chem., Int. Ed.* **2017**, *56*, 9747−9751.

(10) Sun, Q.; Wang, N.; Zhang, T.; Bai, R.; Mayoral, A.; Zhang, P.; Zhang, Q.; Terasaki, O.; Yu, J. Zeolite-Encaged Single-Atom Rhodium Catalysts: Highly-Efficient Hydrogen Generation and Shape-Selective Tandem Hydrogenation of Nitroarenes. *Angew. Chem., Int. Ed.* **2019**, *58*, 18570−18576.

(11) Berguerand, C.; Yarulin, A.; Cárdenas-Lizana, F.; Wärnå, J.; Sulman, E.; Murzin, D. Y.; Kiwi-Minsker, L. Chemoselective Liquid Phase Hydrogenation of 3-Nitrostyrene over Pt Nanoparticles: Synergy with ZnO Support. *Ind. Eng. Chem. Res.* **2015**, *54*, 8659−8669.

(12) Furukawa, S.; Takahashi, K.; Komatsu, T. Well-Structured Bimetallic Surface Capable of Molecular Recognition for Chemoselective Nitroarene Hydrogenation. *Chem. Sci.* **2016**, *7*, 4476−4484.

(13) Serna, P.; Corma, A. Transforming Nano Metal Nonselective Particulates into Chemoselective Catalysts for Hydrogenation of Substituted Nitrobenzenes. *ACS Catal.* **2015**, *5*, 7114−7121.

(14) Macino, M.; Barnes, A. J.; Althahban, S. M.; Qu, R.; Gibson, E. K.; Morgan, D. J.; Freakley, S. J.; Dimitratos, N.; Kiely, C. J.; Gao, X.; Beale, A. M.; Bethell, D.; He, Q.; Sankar, M.; Hutchings, G. J. Tuning of Catalytic Sites in Pt/TiO2 Catalysts for the Chemoselective Hydrogenation of 3-Nitrostyrene. *Nat. Catal.* **2019**, *2*, 873−881.

(15) Mitsudome, T.; Mikami, Y.; Matoba, M.; Mizugaki, T.; Jitsukawa, K.; Kaneda, K. Design of a Silver-Cerium Dioxide Core-Shell Nanocomposite Catalyst for Chemoselective Reduction Reactions. *Angew. Chem., Int. Ed.* **2012**, *51*, 136−139.

(16) Tamura, M.; Yuasa, N.; Nakagawa, Y.; Tomishige, K. Selective Hydrogenation of Nitroarenes to Aminoarenes Using a MoO_X-Modified Ru/SiO_2 Catalyst under Mild Conditions. *Chem. Commun.* **2017**, *53*, 3377−3380.

(17) Wei, H.; Ren, Y.; Wang, A.; Liu, X.; Liu, X.; Zhang, L.; Miao, S.; Li, L.; Liu, J.; Wang, J.; Wang, G.; Su, D.; Zhang, T. Remarkable Effect of Alkalis on the Chemoselective Hydrogenation of Functionalized Nitroarenes over High-Loading Pt/FeO_X Catalysts. *Chem. Sci.* **2017**, *8*, 5126−5131.

(18) Wang, Y.; Qin, R.; Wang, Y.; Ren, J.; Zhou, W.; Li, L.; Ming, J.; Zhang, W.; Fu, G.; Zheng, N. Chemoselective Hydrogenation of Nitroaromatics at the Nanoscale Iron(III)-OH-Platinum Interface. *Angew. Chem., Int. Ed.* **2020**, *59*, 12736−12740.

(19) Zhao, J.; Fang, L.; Fu, J.; Wang, J.; Jiang, Q.; Li, T.; Huang, J. Highly Selective IrMo/TiO_2 Catalyst for Hydrogenation of Nitroarenes. *Mol. Catal.* **2022**, *531*, 112705.

(20) Putaj, P.; Lefebvre, F. Polyoxometalates Containing Late Transition and Noble Metal Atoms. *Coord. Chem. Rev.* **2011**, *255*, 1642−1685.

(21) Hayashi, S.; Shishido, T. High-Density Formation of Metal/Oxide Interfacial Catalytic Active Sites through Hybrid Clustering. *ACS Appl. Mater. Interfaces* **2021**, *13*, 22332−22340.

(22) Hayashi, S.; Endo, S.; Miura, H.; Shishido, T. Highly Active and Durable Rh-Mo-Based Catalyst for the NO-CO-C_3H_6-O_2 Reaction Prepared by Using Hybrid Clustering. *ACS Mater. Au* **2023**, DOI: 10.1021/acsmaterialsau.3c00001.

(23) Takahashi, K.; Yamaguchi, M.; Shido, T.; Ohtani, H.; Isobe, K.; Ichikawa, M. Molecular Modelling of Supported Metal Catalysts: SiO_2-Grafted $[\{(\eta^3\text{-}C_4H_7)_2Rh\}_2V_4O_{12}]$ and $[\{Rh(C_2Me_5)\}_4V_6O_{19}]$ Are Catalytically Active in the Selective Oxidation of Propene to Acetone. *J. Chem. Soc. Chem. Commun.* **1995**, *12*, 1301−1303.

(24) Ichikawa, M.; Pan, W.; Imada, Y.; Yamaguchi, M.; Isobe, K.; Shido, T. Surface-Grafted Metal Oxide Clusters and Metal Carbonyl Clusters in Zeolite Micropores; XAFS/FTIR/TPD Characterization and Catalytic Behavior. *J. Mol. Catal. A Chem.* **1996**, *107*, 23−38.

(25) Hayashi, Y.; Toriumi, K.; Isobe, K. Novel Triple Cubane-Type Organometallic Oxide Clusters: $[MCp^*MoO_4]_4 \bullet nH_2O$ (M = Rh and Ir; Cp* = C_5Me_5; n = 2 for Rh and 0 for Ir). *J. Am. Chem. Soc.* **1988**, *110*, 3666−3668.

(26) Hayashi, Y.; Ozawa, Y.; Isobe, K. Site-Selective Oxygen Exchange and Substitution of Organometallic Groups in an Amphiphilic Quadruple-Cubane-Type Cluster. Synthesis and Molecular Structure of $[(MCp^*)_4V_6O_{19}]$ (M = Rh, Ir). *Inorg. Chem.* **1991**, *30*, 1025−1033.

(27) Yamamoto, T. Assignment of Pre-Edge Peaks in K-Edge x-Ray Absorption Spectra of 3d Transition Metal Compounds: Electric Dipole or Quadrupole? *X-Ray Spectrom.* **2008**, *37*, 572−584.

(28) Shishido, T.; Asakura, H.; Yamazoe, S.; Teramura, K.; Tanaka, T. Structural Analysis of Group V, VI, VII Metal Compounds by XAFS and DFT Calculation. *J. Phys. Conf. Ser.* **2009**, *190*, 012073.

(29) Han, B.; Guo, Y.; Huang, Y.; Xi, W.; Xu, J.; Luo, J.; Qi, H.; Ren, Y.; Liu, X.; Qiao, B.; Zhang, T. Strong Metal-Support Interactions

between Pt Single Atoms and TiO_2. *Angew. Chem., Int. Ed.* **2020**, *59*, 11824−11829.
(30) Xiong, M.; Wang, G.; Zhao, S.; Lv, Z.; Xing, S.; Zhang, J.; Zhang, B.; Qin, Y.; Gao, Z. Engineering of Platinum-Oxygen Vacancy Interfacial Sites in Confined Catalysts for Enhanced Hydrogenation Selectivity. *Catal. Sci. Technol.* **2022**, *12*, 2411−2415.
(31) Yang, X.-F.; Wang, A.; Qiao, B.; Li, J.; Liu, J.; Zhang, T. Single-Atom Catalysts: A New Frontier in Heterogeneous Catalysis. *Acc. Chem. Res.* **2013**, *46*, 1740−1748.
(32) Prasomsri, T.; Nimmanwudipong, T.; Román-Leshkov, Y. Effective Hydrodeoxygenation of Biomass-Derived Oxygenates into Unsaturated Hydrocarbons by MoO_3 Using Low H_2 Pressures. *Energy Environ. Sci.* **2013**, *6*, 1732−1738.
(33) Kuwahara, Y.; Yoshimura, Y.; Haematsu, K.; Yamashita, H. Mild Deoxygenation of Sulfoxides over Plasmonic Molybdenum Oxide Hybrid with Dramatic Activity Enhancement under Visible Light. *J. Am. Chem. Soc.* **2018**, *140*, 9203−9210.
(34) Tamura, M.; Tokonami, K.; Nakagawa, Y.; Tomishige, K. Selective Hydrogenation of Crotonaldehyde to Crotyl Alcohol over Metal Oxide Modified Ir Catalysts and Mechanistic Insight. *ACS Catal.* **2016**, *6*, 3600−3609.
(35) He, S.; Xie, L.; Che, M.; Chan, H. C.; Yang, L.; Shi, Z.; Tang, Y.; Gao, Q. Chemoselective Hydrogenation of α,β-Unsaturated Aldehydes on Hydrogenated MoO_x Nanorods Supported Iridium Nanoparticles. *J. Mol. Catal. A Chem.* **2016**, *425*, 248−254.
(36) Wang, L.; Guan, E.; Zhang, J.; Yang, J.; Zhu, Y.; Han, Y.; Yang, M.; Cen, C.; Fu, G.; Gates, B. C.; Xiao, F.-S. Single-Site Catalyst Promoters Accelerate Metal-Catalyzed Nitroarene Hydrogenation. *Nat. Commun.* **2018**, *9*, 1362.
(37) Ankudinov, A. L.; Ravel, B.; Rehr, J. J.; Conradson, S. D. Real-space multiple-scattering calculation and interpretation of x-ray-absorption near-edge structure. *Phys. Rev. B* **1998**, *58*, 7565−7576.

https://doi.org/10.1021/acsorginorgau.3c00017
ACS Org. Inorg. Au 2023, 3, 283−290